BRAIN
A JOURNAL OF NEUROLOGY

Myelin-associated glycoprotein gene mutation causes Pelizaeus-Merzbacher disease-like disorder

Alexander Lossos,[1],* Nimrod Elazar,[2],* Israela Lerer,[3],* Ora Schueler-Furman,[4] Yakov Fellig,[5] Benjamin Glick,[6] Bat-El Zimmerman,[3] Haim Azulay,[5] Shlomo Dotan,[7] Sharon Goldberg,[7] John M. Gomori,[8] Penina Ponger,[1] J. P. Newman,[1] Hodaifah Marreed,[3] Andreas J. Steck,[9] Nicole Schaeren-Wiemers,[9] Nofar Mor,[2] Michal Harel,[10] Tamar Geiger,[10] Yael Eshed-Eisenbach,[2] Vardiella Meiner,[3],* and Elior Peles[2]

*These authors contributed equally to this work.

Pelizaeus-Merzbacher disease is an X-linked hypomyelinating leukodystrophy caused by mutations or rearrangements in *PLP1*. It presents in infancy with nystagmus, jerky head movements, hypotonia and developmental delay evolving into spastic tetraplegia with optic atrophy and variable movement disorders. A clinically similar phenotype caused by recessive mutations in *GJC2* is known as Pelizaeus-Merzbacher-like disease. Both genes encode proteins associated with myelin. We describe three siblings of a consanguineous family manifesting the typical infantile-onset Pelizaeus-Merzbacher disease-like phenotype slowly evolving into a form of complicated hereditary spastic paraplegia with mental retardation, dysarthria, optic atrophy and peripheral neuropathy in adulthood. Magnetic resonance imaging and spectroscopy were consistent with a demyelinating leukodystrophy. Using genetic linkage and exome sequencing, we identified a homozygous missense c.399C>G; p.S133R mutation in *MAG*. This gene, previously associated with hereditary spastic paraplegia, encodes myelin-associated glycoprotein, which is involved in myelin maintenance and glia-axon interaction. This mutation is predicted to destabilize the protein and affect its tertiary structure. Examination of the sural nerve biopsy sample obtained in childhood in the oldest sibling revealed complete absence of myelin-associated glycoprotein accompanied by ill-formed onion-bulb structures and a relatively thin myelin sheath of the affected axons. Immunofluorescence, cell surface labelling, biochemical analysis and mass spectrometry-based proteomics studies in a variety of cell types demonstrated a devastating effect of the mutation on post-translational processing, steady state expression and subcellular localization of myelin-associated glycoprotein. In contrast to the wild-type protein, the p.S133R mutant was retained in the endoplasmic reticulum and was subjected to endoplasmic reticulum-associated protein degradation by the proteasome. Our findings identify involvement of myelin-associated glycoprotein in this family with a disorder affecting the central and peripheral nervous system, and suggest that loss of the protein function is responsible for the unique clinical phenotype.

1 Department of Neurology and Agnes Ginges Centre for Human Neurogenetics, Hebrew University-Hadassah Medical Centre, Jerusalem, Israel
2 Department of Molecular Cell Biology, Weizmann Institute of Science, Rehovot, Israel
3 Department of Genetics and Metabolic Diseases, Hebrew University-Hadassah Medical Centre, Jerusalem, Israel
4 Department of Microbiology and Molecular Genetics, Institute for Medical Research Israel-Canada, Faculty of Medicine, Hebrew University, Jerusalem, Israel
5 Department of Pathology, Hebrew University-Hadassah Medical Centre, Jerusalem, Israel
6 Paediatric Neuromuscular Service, Alyn Paediatric Rehabilitation Centre, Jerusalem, Israel
7 Department of Ophthalmology, Hebrew University-Hadassah Medical Centre, Jerusalem, Israel

8 Department of Radiology, Hebrew University-Hadassah Medical Centre, Jerusalem, Israel
9 Department of Biomedicine, University Hospital Basel, University of Basel, Switzerland
10 Department of Human Molecular Genetics and Biochemistry, Sackler Faculty of Medicine, Tel Aviv University, Tel Aviv, Israel

Correspondence to: Vardiella Meiner, MD,
Department of Genetics and Metabolic Diseases,
Hebrew University-Hadassah Medical Centre,
PO Box 12000 Jerusalem,
91120 Israel
E-mail: vmeiner@hadassah.org.il

Correspondence may also be addressed to: Alexander Lossos,
MD, Department of Neurology,
Hebrew University-Hadassah Medical Centre,
PO Box 12000 Jerusalem,
91120 Israel
E-mail: also@hadassah.org.il

Elior Peles,
Department of Molecular Cell Biology,
Weizmann Institute of Science,
Rehovot, Israel
E-mail: peles@weizmann.ac.il

Introduction

Pelizaeus-Merzbacher disease (PMD; OMIM #312080) is the prototype hypomyelinating leukodystrophy (HLD1) classically presenting in infancy with nystagmus, jerky head movements, hypotonia and developmental delay evolving into spastic tetraplegia with optic atrophy and variable movement disorders (Hobson and Garbern, 2012). It is an X-linked disorder caused by mutations or rearrangements in the *PLP1* gene encoding two alternatively spliced isoforms of an integral membrane proteolipid protein (PLP/DM20), a major component of the CNS and a minor one of the peripheral nervous system (PNS) compact myelin (Han *et al.*, 2013). A clinically similar phenotype associated with hypomyelination but not linked to *PLP1* is termed Pelizaeus-Merzbacher-like disease (PMLD) (Hobson and Garbern, 2012) and classified with a genetically heterogeneous group of HLD (Pouwels *et al.*, 2014). PMLD1 (OMIM #608804), classified as HLD2, accounts for 8% of such patients (Henneke *et al.*, 2008). It is caused by recessive mutations in *GJC2*, encoding gap junction protein gamma 2 or connexin 47 expressed in oligodendrocytes and involved in oligodendrocyte-astrocyte channelling and in the maintenance of myelin (Orthmann-Murphy *et al.*, 2009).

Additional disorders resembling PMD are associated with delayed myelination, as in *SLC16A2*-related dysfunction of monocarboxylate thyroid hormone transporter 8 (Vaurs-Barriere *et al.*, 2009) (OMIM #300523), or with hypomyelination secondary to a neuronal or axonal process, as in a presumed *AIMP1*-related dysregulation of the neurofilament network in HLD3 (Feinstein *et al.*, 2010; Pouwels *et al.*, 2014) (OMIM #260600), in *HSPD1*-related compromise of the mitochondrial chaperonin HSP60 in HLD4 (Magen *et al.*, 2008; Pouwels *et al.*, 2014) (OMIM #612233), and occasionally in *TUBB4A*-related tubulin beta-4A dysfunction in HLD6 (Miyatake *et al.*, 2014; Shimojima *et al.*, 2015) (OMIM #612438).

We report the clinical, molecular and cell biological data of a multiplex family with early PMD-like disorder slowly evolving into a form of hereditary spastic paraplegia (HSP) associated with demyelination due to a homozygous loss-of-function mutation in *MAG*, the gene previously reported in HSP (Novarino *et al.*, 2014). Encoded protein, known as myelin-associated glycoprotein MAG, is a cell adhesion molecule that belongs to the immunoglobulin (Ig) superfamily of proteins enriched in myelinating glial cells and involved in glia-axon interactions.

Materials and methods

Patients

Since 2009, we have evaluated three affected siblings of a consanguineous family of Palestinian Arab origin (Fig. 1A). Of the living clinically unaffected family members, 13 were available for examination. The family was registered in the Israeli HSP Database in 2009. Clinical diagnosis and a prospective
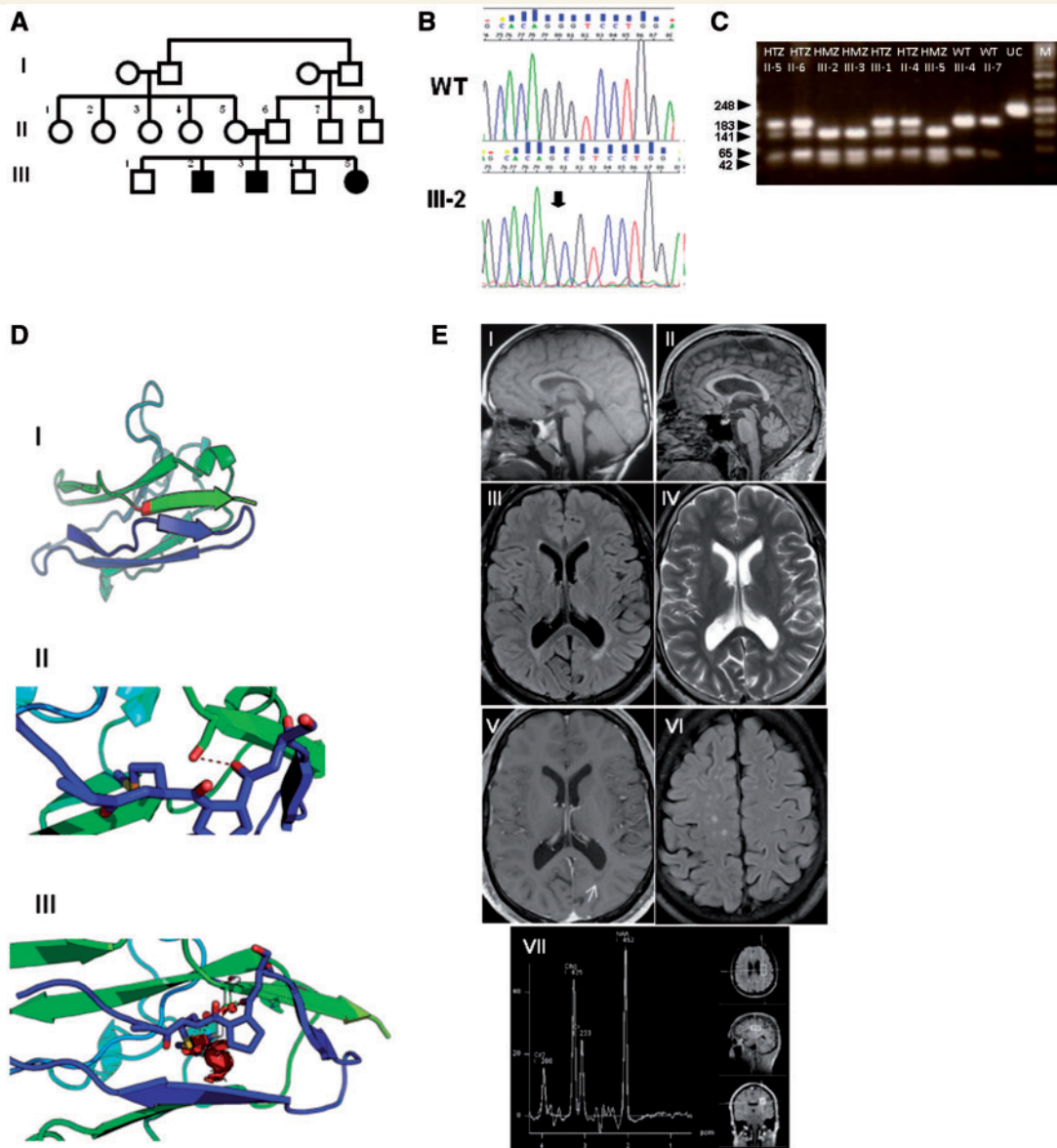
Figure 1 **Homozygous c.399C > G mutation in *MAG* in the autosomal recessive PMD-like disorder**. (**A**) Pedigree of the family. Circles represent females and squares males. Filled symbols indicate affected individuals and double lines consanguinity by descent. (**B**) DNA sequencing identified a c.399C > G, p.S133R mutation in *MAG*. *Upper* panel shows wild-type sequence (WT) and *lower* panel shows affected homozygous Patient III-2. (**C**) Restriction-based analysis of individuals from the extended family. PCR products were digested with AvaII resulting in a wild-type (183 + 65 bp) and a mutant allele (141 + 65 + 42 bp). M = marker; UC = uncut; HTZ = heterozygote; HMZ = homozygote, with the letters designating position in the pedigree. (**D**) Modelling of the p.S133R mutation effect on MAG stability and structure. Structural model of the first Ig-like domain (residues 22–139) suggests that S133 points into the core of this domain to form hydrogen bonds with a neighbouring proline residue. Mutation to arginine will create strong clashes leading to unfolding and destabilization of the protein. (**I**) Overall model of the first Ig-like domain of MAG. S133 (in red) is located in the c-terminal strand of the first Ig-like domain (in green), adjacent to the n-terminal strand of this (in blue). Interaction between these two strands holds the domain together. (**II**) Close-up of the S133 position (green central residue in sticks representation) and its surrounding showing a potential hydrogen bond formed with a neighboring backbone, P27 at the N-terminal of the Ig-like domain (dashed lines). (**III**) Mutation of serine to arginine (in white) at position 133 leads to strong clashes (in red) and may cause opening of the sheet to its unfolding and misfolding. (**E**) Representative imaging findings. Cerebral MRI in Patient III-2 at age 7 (**I**) and 25 (**II–V** and **VII**) years and in Patient III-3 at age 24 (**VI**) showing mild progressive atrophy of the optic chiasm, corpus callosum and cerebellum on T_1-weighted images (**I** and **II**), a periventricular rim of the cerebral white matter hyperintensity on FLAIR (**III**) and T_2-weighted (**IV**) images, which appears hypointense on T_1(+ Gd)-weighted images (**V**, arrow), and scattered foci of hyperintensity on FLAIR-weighted images (**VI**). Areas of the unaffected cerebral white matter appear of a normal signal. (**VII**) Cerebral ^{1}H-magnetic resonance spectroscopy (echo time 135) spectrum at the centrum semiovale showing an increase in choline peak.

follow-up were performed using the clinical chart (http://spatax.wordpress.com/downloads/) developed by the international SPATAX (spastic paraplegia and ataxia) network (coordinator: A. Durr, MD, PhD). For cognitive evaluation and assessment of the intelligence quotient we used Mini-Mental State Examination (Folstein *et al.*, 1975) and the Test for Non-Verbal Intelligence (TONI-2), a language-free tool for obtaining predicted non-verbal intelligence scores (www.agsnet.com/). The study was approved by the institutional and national review boards. Informed consent was obtained prior to enrolment from all the participants.

Autozygosity mapping and linkage analysis

Because of the parental consanguinity, we determined shared homozygous regions using genome-wide linkage analysis with the Affymetrix® Gene-Chip Human Mapping 250K Nsp Array. Data handling, evaluation and the statistical analysis were performed using HomozygosityMapper (Seelow *et al.*, 2009). To assess and confirm segregation with the phenotype, we used selected short tandem repeat (STR) markers for genotyping the remaining family members (details available upon request).

Whole exome sequencing

For whole exome sequencing, DNA obtained from Patient III-2 was fragmented, end paired, adenylated and ligated to adapters. Exome capture and sequencing was performed with the Agilent SureSelect 38 Mb All Exon Hybridization Array. The SureSelect protocol was used to prepare libraries for paired-end sequencing on an Illumina HiSeq 2000 platform with mean depth coverage of $30\times$. The sequenced reads were aligned, and variant calling was performed with the October 2011 release of DNAnexus software with the human genome assembly hg19 (GRCh37) as reference. The raw list of variants was filtered to exclude variants present in the dbSNP129, in the 'HapMap' and in the '1000 Genomes' databases. Rigorous filtering based on global (minor allele frequency) MAF < 1%, predicted functional consequence, and sequence conservation left us with sequence variants of interest that were validated and verified using Sanger sequencing and restriction fragment length polymorphism (RFLP) analysis.

Mutation analysis

For the *MAG* c.399C>G; p.S133R mutation (NM_002361.3), PCR product (248 bp; amplified by forward 5'-GAAACTGC ACCCTCCTGCT-3' and reverse 5'-CAAATCAGCACCTCCC AGATC-3') was digested with AvaII (Promega) as per manufacturer's protocol and run on NuSieve® agarose (3:1%) gel leading to the detection of a normal and a mutant allele (183 + 65 bp and 141 + 65 + 42 bp, respectively).

For the *PLP1* c.594C>A variant (NM_000533.3), we used AlwNI restriction enzyme analysis with the primers PLP1EX5F-5'-TGGTTTTAATGTCTGGCACA-3' and PLP1 EX5R-5'-CTCATAATCACCACCCTCCTT-3'. *PLP1* cDNA was analysed with the primers PLP1-290F-5'-AGGCAGATC TTTGGCGACTA-3' and PLP1-800R-5'-GTGAGCAGGGA AACCAGTGT-3'. PCR products were run on agarose gel and visualized under UV illumination.

Expression of wild-type and mutant MAG

Human *MAG* was cloned by reverse transcription-PCR from total RNA of human femoralis cDNA and was subcloned into pβ-actin-ECGFP exchanging the ECGFP sequence (pβ-actin-hSMAG), or into the same vector upstream of the EGFP (pβ-actin-hSMAG-GFP) (Erb *et al.*, 2003). c.399C>G mutation was generated by PCR on pβ-actin-hSMAG as template. A forward primer (5'-CTCCATCTCCAGCCTCGGG-3') and a reverse primer (5'-GGTGTTGACGATATCCAGGACCCTGT GCTCTGAGAAGGTGTAC-3') containing the mutation and a neighbouring endogenous EcoRV site were used. A HindIII–EcoRV-digested PCR fragment was ligated into the template plasmid in the same site to generate pβ-actin-hSMAG-S133R. The pβ-actin-hSMAG-S133R-GFP was generated by replacing the HindIII–EcoRV fragment of hSMAG-GFP with the one obtained from pβ-actin-hSMAG-S133R. Plasmids containing myc-tagged versions of wild-type and mutant *MAG* were made by PCR cloning of the corresponding genes into pMX vector (Addgene). The latter plasmid was also used to generate viral vectors containing GFP-tagged proteins. The open reading frame of all constructs was confirmed by DNA sequencing. Transfection of HEK-293T, COS7 and Schwann cells were done using CaPO$_4$, Lipofectamine™ (Invitrogen), and Lipofectamine™ 2000 reagent (Invitrogen), respectively. Lentiviral stocks were generated by CaPO$_4$-transfection of phoenix packaging cells (Invitrogen). Rat Schwann cells and oligodendrocyte precursor cells were cultured as described (Eshed *et al.*, 2005).

Antibodies and immunofluorescence labelling

We used mouse monoclonal antibody (MAb) D3A2G5 against the extracellular domain of human MAG (Burger *et al.*, 1990), a monoclonal anti-mouse MAG (clone MAb 513, EMD Millipore), rabbit polyclonal anti-MAG (H-300; Santa Cruz Biotechnologies), and polyclonal anti-L-MAG (Heape *et al.*, 1999, kindly obtained from Dr A. Heape, University of Oulu, Finland). For immunohistochemical staining of the sural nerve sample, we used anti-MAG antibody against amino acids 1–300 mapping near the N-terminus of human MAG (H-300; sc-15324, Santa Cruz Biotechnology Inc, 1:50, and NF-Neurofilament Protein, Clone 2F11, Dako, 1:500. Other antibodies included mouse anti-calnexin (MAb3126; EMD Millipore), mouse monoclonal antibody to vesicle docking protein p115 (kindly provided by Dr S. Lev, Weizmann Institute, Israel), rabbit anti-VapB (K-16; Santa Cruz Biotechnologies), and rabbit polyclonal antibody to Caspr (Peles *et al.*, 1997). Fluorophore-coupled secondary antibodies included 488- coupled anti-rabbit and mouse IgG (Invitrogen), Cy3-coupled anti-rabbit and anti-mouse (Jackson Laboratories). Immunofluorescence labelling was carried out essentially as described (Spiegel *et al.*, 2007). Fluorescence images were obtained using an Axioskop2 microscope equipped with an ApoTom imaging system (Carl Zeiss) fitted with a Hamamatsu ORCA-ER CCD camera. Images were acquired and processed using the Zen2012 (Carl Zeiss) and Photoshop software (Adobe).

Structural protein modelling

Structural model of MAG and the corresponding MAG-S133R mutant was generated using the HHpred tool (Söding, 2005), to identify structural templates for homology modelling, and the I-Tasser tool (Roy *et al.*, 2010), to create the model using a longer domain definition than predicted earlier by other tools (May *et al.*, 1998). The structure of a similar protein sialoadhesin (Protein Data Bank code 1qfo) with a 26% sequence identity and 66% sequence similarity (May *et al.*, 1998) served as the basis for this model.

Immunoprecipitation and western blot analysis

Immunoprecipitation, sodium dodecyl sulphate-polyacrylamide gel electrophoresis (SDS-PAGE) and western blotting were done as described (Spiegel *et al.*, 2007) with the exception that the chemiluminescence signal was detected using the ChemiDoc MP System (Bio-Rad). Deglycosylation and removing of high mannose structures was achieved by incubating the denatured immunocomplexes with endoglycosidase H (New England Biolabs) for 1 h at 37°C. Co-immunoprecipitation of endogenously expressed proteins was performed using HEK-293T cells either incubated with dimethyl sulphoxide or incubated with the indicated amount of bortezomib overnight. Cells were solubilized in Triton™ X-100 containing buffer, incubated with GFP-Trap®-Agarose (ChromoTek) followed by western blot analysis (Peles *et al.*, 1997). When indicated, protein synthesis was stopped by the addition of cyclohexamide to a final concentration of 50 μg/ml for various times. Cells were then washed in phosphate-buffered saline, lysed and total protein lysates were subjected to western blot analysis. Cell surface biotinylation was done as described (Gollan *et al.*, 2003).

Proteomics sample preparation and mass spectrometry analysis

Cells were lysed with 1% NP40, 150 mM NaCl in 50 mM Tris HCl pH 7.6 buffer supplemented with protease inhibitors. Protein from each sample (5 mg) was mixed with GFP-Trap®-Agarose (ChromoTek) for 2 h at 4°C. Samples were washed three times with the same buffer containing 0.05% NP40 followed by three washes without NP40. Proteins were reduced with 1 mM dithiothreitol in 2 M urea and subsequently alkylated with 5 mM iodoacetamide. On-bead protein digestion was performed with sequencing grade-modified trypsin (Promega) and peptides were acidified with trifluoroacetic acid (TFA) followed by purification on C18 (stageTips). Liquid chromatography-mass spectrometry (LC-MS/MS) analysis was performed on the EASY-nLC1000 UHPLC system (Thermo Scientific) coupled to the Q-Exactive Plus mass spectrometers (Thermo Scientific) via the EASY-Spray™ ionization source. Peptides were loaded onto 50 cm long EASY-Spray™ PepMap columns (Thermo Scientific) with 140-min gradient using buffer A (0.1% formic acid) and separated using a 7–28% buffer B (80% acetonitrile, 0.1% formic acid). All mass spectrometry measurements were done in a data-dependent mode using a top-10 method. Raw mass spectrometry files were analysed with MaxQuant version 1.5.0.36 and the Andromeda search engine integrated into the same version (Cox *et al.*, 2011). MS/MS spectra were searched against the UniprotKB database. Quantification was performed using the label-free algorithm MaxLFQ (Cox *et al.*, 2014).

All bioinformatics analyses were performed on log2 LFQ intensity values. Data analysis was performed after filtering for valid values in at least two samples in one group (empty vector/wild-type/S133R mutant). Statistical tests and calculations were done using the Perseus program. To identify potential interactors, Student's *t*-test was performed between empty vector triplicate and either wild-type or mutant triplicates with permutation-based false discovery rate (FDR) < 0.05 and S0 = 1.5 and resulted in a list of 1010 proteins with higher intensities in the MAG samples. A second Student's *t*-test (FDR = 0.05, S0 = 1.5) was performed on these proteins to distinguish between the wild-type and mutant binders. Hierarchical clustering was done after z-score normalization of the proteins, and was based on Euclidean distances between averages. Protein networks were constructed in the string database and visualized in Cytoscape. Fisher exact tests were done with a Benjamini–Hochberg FDR threshold of 0.02.

Results

Patients manifest complicated hereditary spastic paraplegia

The main clinical findings at initial examination and the available documented medical history are summarized in Table 1. In short, the patients were born after uneventful pregnancies and labour and, except for Patient III-2 who had transverse limb defect affecting phalanges in three fingers of his right hand, none had dysmorphic features. Head circumferences were within normal limits. Early developmental and speech delay were noticed soon after birth with initiation of supported gait at age 4–5 years and slow but progressive deterioration to walker and wheelchair over a period of 15 years, despite physiotherapy. Borderline-to-mild mental retardation was documented in all three siblings. They attended special school, obtained basic reading and writing skills, and achieved partial independence in basic daily activities. Based on the combination of early ocular and neurological findings (Table 1), initial diagnosis of PMD was raised by age 5 years (B.G.).

On examination, patients had spastic dysarthria and moderate-to-severe spastic paraparesis with hyporeflexia in the arms and knees, reduced (Patient III-5) or absent (Patients III-2 and III-3) ankle reflexes and bilateral extensor plantar response. Muscle tone in the arms was only mildly increased and was associated with dysmetria. Reduced deep tendon reflexes together with distal leg atrophy and distal vibration sensory loss suggested an associated peripheral neuropathy. Patients displayed mild psychomotor slowing, intact short-term verbal memory, full orientation in all domains, and scored in the range of mild (Patient III-5) to borderline (Patients III-2 and III-3) mental retardation.

Table 1 Clinical findings at the initial evaluation of the siblings with a homozygous c.399C>G mutation in *MAG*

Patient	III-2	III-3	III-5
Sex	Male	Male	Female
Age at: (years)			
Initial evaluation	23	22	17
Current	28	26	21
Age at documented finding (years)			
Nystagmus	Days	1	1
Head nodding	1	–	–
Hypotonia	Days	1	1
Hypo-areflexia	4	1	4
Spasticity	4	9	9
Pyramidal signs	4	9	4
Developmental delay	+	+	+
Supported walking	5	4	5
Walking with walker	10	9	9
Wheelchair-bound	20	19	–
Cognitive			
MMSE	25/30	23/30	24/30
IQ	71	76	61
Ocular right/left			
Visual acuity	0.1/FC	0.2/0.2	0.16/0.16
Refraction	Hypermetropia, astigmatism	Hypermetropia, astigmatisms	High hypermetropia, astigmatism
IOP (normal <21 mm Hg)	31/32	10/10	10/10
RAPD	R	–	–
Oculomotor	Nystagmus	Nystagmus	Nystagmus
Optic nerve	Pale excavation/central pale excavation	Temporal pallor/temporal pallor	Temporal pallor/temporal pallor
Spastic dysarthria	Moderate	Moderate	Mild
Spastic paraparesis (severity)	Severe	Severe	Moderate
Hypo-areflexia	+	+	+
Extensor plantar response, right/left	+/+	+/+	+/+
Dysmetria	Mild	Mild	Mild
Distal sensory deficit	Vibration	Vibration	Vibration
Distal leg atrophy	+	+	+

MMSE = Mini-Mental State Examination; R = right; L = left; FC = finger counting; IOP = intraocular pressure; RAPD = relative afferent papillary defect.

Formal neuro-ophthalmological examination (Table 1) revealed similar findings in all three siblings, including horizontal nystagmus and optic nerve atrophy with reduced visual acuity, visual field defect, and thinning of the peri-papillary retinal ganglion cell fibres (Supplementary Table 1). In addition, all had hypermetropia and astigmatism, and Patient III-2 had primary open angle glaucoma well-controlled with locally applied medications. Recorded visual-evoked potentials were of significantly low amplitude and of prolonged latency, more in the older siblings (Supplementary Table 1). Brainstem auditory-evoked responses were of delayed latency but a recognizable wave pattern in all three siblings.

Over a period of 4 years, all three siblings were available for follow-up examinations, showing a very slow progression of their functional motor disability and of the clinical findings.

Metabolic screening and EEG were normal in Patient III-2. Peripheral nerve conduction study (Supplementary Table 1) demonstrated in the elder siblings, prolonged distal motor latencies with normal or borderline compound motor action potentials and reduced motor and sensory velocities, indicating motor and sensory peripheral neuropathy. There were no temporal dispersion or conduction blocks.

Cerebral MRI (Supplementary Table 1) demonstrated bilateral optic nerve atrophy accompanied by mild corpus callosum and cerebellar atrophy. In addition, there was a rim of predominantly posterior cerebral periventricular and subtle pontine white matter T_2/FLAIR-hyperintensity, and rare scattered foci of subcortical white matter hyperintensity (Fig. 1E). Areas of unaffected cerebral white matter appeared of a normal signal, suggesting a normal myelination pattern. Mild ventricular dilatation was also noted, likely the result of white matter volume loss. Although these findings were similar in all three siblings, they tended to be more pronounced in the older ones. Furthermore, comparison with a study from 18 years earlier in Patient III-2 revealed slow progression of all findings. Single volume ^{1}H-magnetic resonance spectroscopy obtained with PRESS acquisition at the centrum semiovale (Fig. 1E) revealed elevated ratios of choline to creatine and to N-acetyl aspartate at a long (135 ms) echo time,

particularly in the older siblings (Supplementary Table 1). Taken together, these findings were consistent with a slowly progressive leukodystrophy of a demyelinating rather than a hypomyelinating pattern (Bizzi *et al.*, 2008).

At age 9 years, Patient III-2 was evaluated elsewhere. Left sural nerve biopsy performed at that time was interpreted as normal. Revision of paraffin embedded sections, epoxy resin embedded semi-thin sections and electron microscopy (Fig. 2) did not reveal significant alterations, except for rare ill-formed onion-bulb structures and apparent minimal loss of axon-glia interaction in rare myelinated axons, although traction or tearing artefact cannot not be excluded. There was no 'wide-spaced' myelin formation and no apparent decrease in axonal density. Although subtle, these features may indicate minimal demyelination.

Molecular analysis identifies c.399C > G; p.S133R mutation in *MAG*

Autozygosity mapping in Patients III-2 and III-3 (Fig. 1A) yielded four shared homozygous regions encompassing the following chromosomal regions: chr11:47993662–50299865, chr11:50300221–56027727, chr19:13552763–35976171, and chr18: 45 667 057–67599516 (build hg19). To narrow these candidate regions, we performed segregation analysis using polymorphic microsatellites corresponding to these shared loci, which ruled out chromosome 18 and chromosome 11 regions as potential candidate options. We remained with a single 21 Mb homozygous region corresponding to chromosome 19 (15244658–35976171) encompassing 234 protein-coding genes and a total of 1350 exons.

In light of this large number of genes, we elected to perform whole exome sequencing in Patient III-2. The number of called variants [insertion/deletions (Indels) and single nucleotide variations (SNVs)] was 108 357. Of these variants, 878 were homozygous located in the linked non-excluded region on chromosome 19. Filtering this group resulted in 190 coding variants that were all common and frequently found in the published and in-house variant databases (EVS, 1000 genomes, HapMap) except for a unique variant in the *MAG* gene on chromosome 19:35786868. A silent variant rs2301600 in this codon is a common SNP; however, affected individuals in this family carried a missense change c.399C > G, p.S133R (Fig. 1B). *In silico* analyses with several pathogenicity prediction programs predicted the amino acid substitution to be tolerated by SIFT yet damaging to the protein function using PolyPhen-2 and MutationTaster. Restriction-based analysis demonstrated perfect segregation in the extended family and only the three patients were homozygotes for the mutation (Fig. 1C). This variant was never reported in the database generated by the Exome Aggregation Consortium (ExAC), Cambridge, MA (http://exac.broadinstitute.org) (December, 2014). Serine at position 133 is moderately conserved all the way down to the zebrafish in which a similar polar

neutral amino acid is found. Screening 192 anonymous chromosomes from a similar ethnic background did not reveal any carrier for the mutation.

Because of a PMD-like phenotype, we extensively searched for potential variants in the *PLP1* gene. A single variant on chromosome X, 103 042 867 predicted to cause a silent change (c.594C > A; p.Gly198Gly), was further analysed to assess potential splicing effect. This variant did not segregate with the phenotype and, although shared by the two affected brothers Patients III-2 and III-3, was not detected in their affected sister, Patient III-5. Furthermore, *PLP1* cDNA did not differ in size between the three patients and normal controls, and we concluded that the disease phenotype is not influenced by this variant. We did not identify potential disease-causing variants in the HLD-causing genes *AIMP1*, *GJC2*, *HSPD1*, *TUBB4A*, *FAM126A* and *RARS*.

p.S133R mutation is predicted to affect the structure of MAG

The p.S133R is located at the end of the first of five Ig-like domains (Letunic *et al.*, 2012). To evaluate the structural importance of the affected S133 residue, we generated a structural model of 118 residues (22–139) showing that S133 points into the protein core to form hydrogen bonds with the backbone of residues at the beginning of the Ig-like domain (Fig. 1D). This interaction is also observed in the solved homologue structures and could explain the rather unusual burial of a polar residue in the core. Position 133 is located within the last strand of the Ig-like domain and is inserted between two additional strands to form a beta-sheet, including a bulge of different sizes just prior to 133 (Fig. 1D).

The p.S133R mutation results in the replacement of a small serine with a much larger arginine, thereby disrupting this domain and leading to a significant destabilization of the protein (Fig. 1D). In addition, this mutation could also affect glycosylation, as it is located in the vicinity of the R118, a sialic acid binding site in the same domain.

p.S133R mutation affects the post-translational processing and folding of MAG

To further examine consequences of the mutation on the biochemical characteristics of MAG, we prepared constructs that direct the expression of human MAG or human MAG carrying the S133R mutation (MAG-S133R). In addition, we cloned human MAG or MAG-S133R upstream of EGFP or a myc-tag. Western blot analysis of COS7 cells transfected with the wild-type constructs revealed the presence of multiple MAG or MAG-GFP glycoforms, whereas MAG or MAG-GFP containing the S133R mutation appeared as a single band (Fig. 3A), indicating that the substitution of serine at position 133 to arginine affected the post-
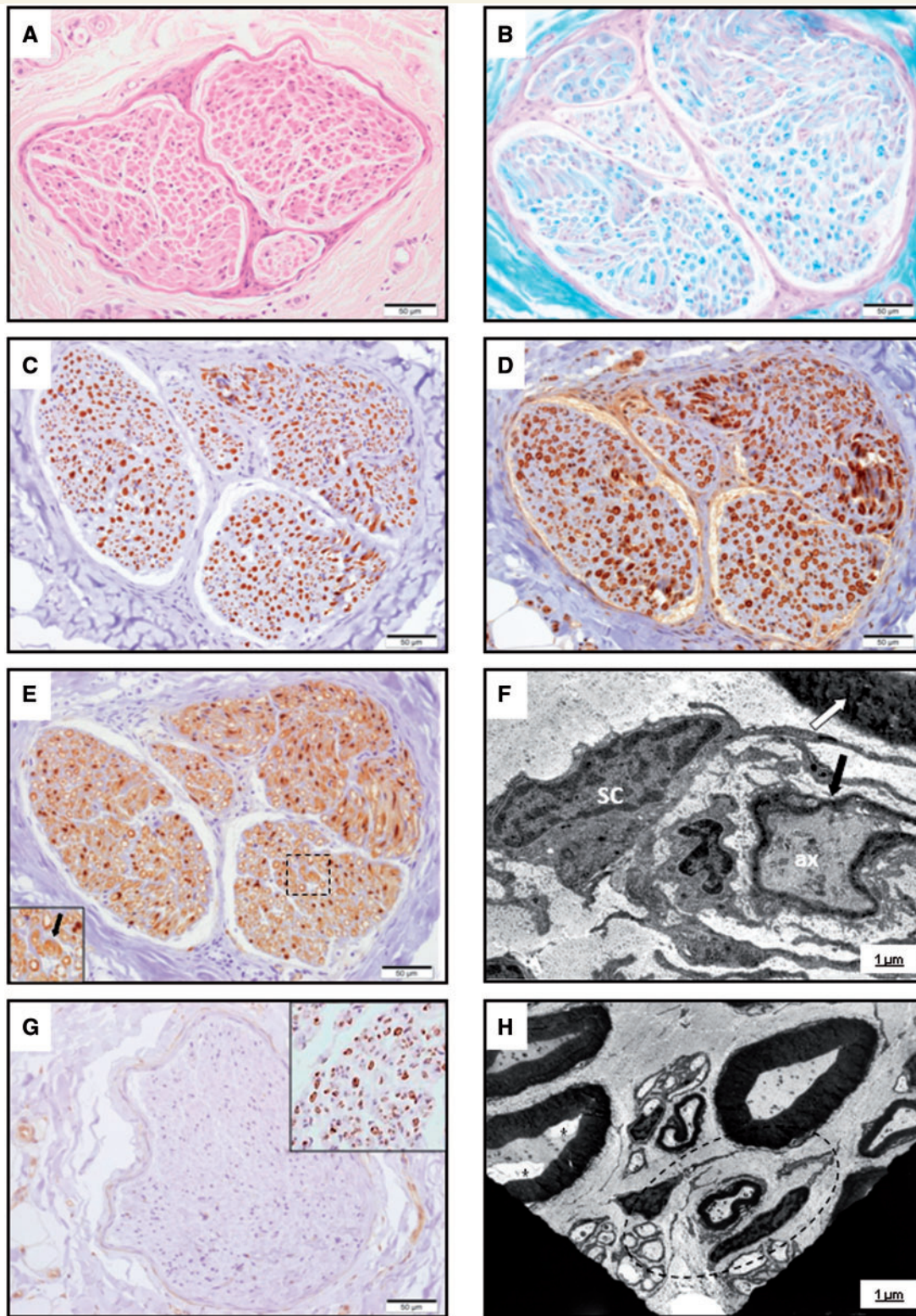
Figure 2 Sural nerve biopsy findings in Patient III-2. Paraffin embedded sections stained with haematoxylin and eosin (**A**), Luxol Fast blue–periodic acid–Schiff (**B**), and with immunohistochemical stains for neurofilament (**C**), MBP (**D**), S-100 protein (**E**) and MAG (**G**), as well as electron-microscopy (**F** and **H**) did not reveal remarkable alterations, except for rare ill-formed onion-bulb structures, noted only on S-100 stained section (**E**, inset, arrow) and electron-microscopy (**F**, **H**, encircled). Myelin sheath of the affected nerve appears relatively thin (**F**, black arrow) as opposed to myelin sheath of most axons (**F**, white arrow). Possible minimal loss of axon-glia interaction (**H**, asterisks) was noted in rare myelinated axons, but traction/tearing artefact cannot be excluded. There was complete absence of myelin sheath staining for MAG (**G**), compared to a normal control (**G**, inset). SC = Schwann cell nucleus; ax = axon.
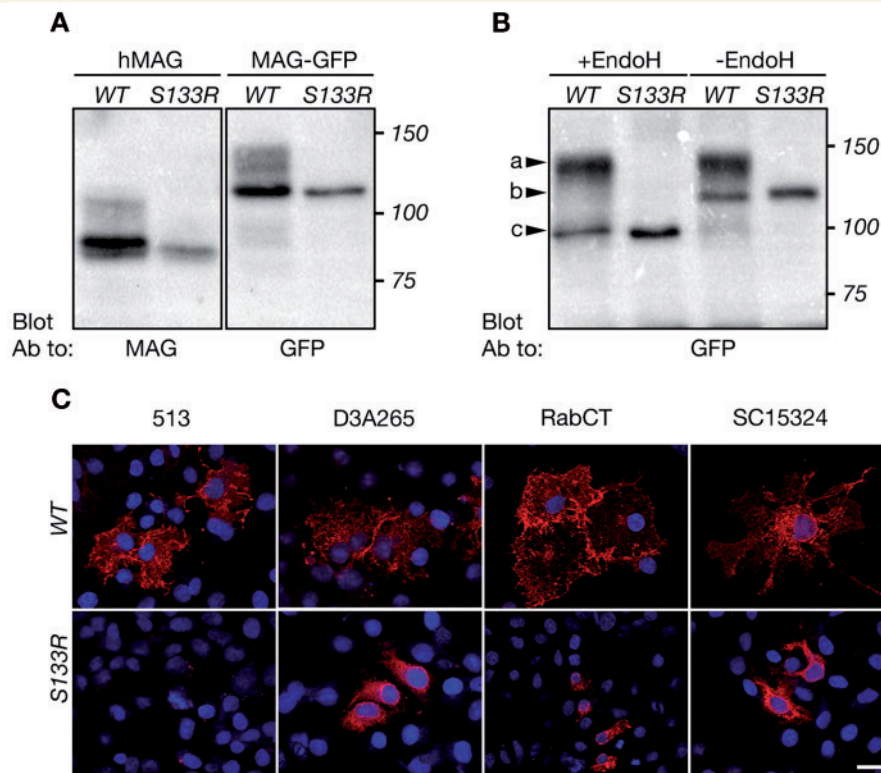
Figure 3 Characterization of the MAG-S133R mutant. (A) Expression of the wild-type (*WT*) and mutant (*S133R*) human MAG (hMAG) and of these proteins fused to GFP (MAG-GFP) in HEK-293 cells. Western blot analysis was done on total cell lysates using antibodies to MAG or GFP. The location of molecular weight markers is shown in kDa on the right. **(B)** MAG-S133R mutant lacks complex glycans. Immunocomplexes of wild-type (*WT*) and mutant (*S133R*) MAG-GFP expressed in HEK-293 cells were left untreated or treated with endoglycosidase H (EndoH), which cleaves asparagine-linked mannose rich oligosaccharides but not highly processed complex oligosaccharides from glycoproteins. Western blot analysis was done using an antibody to GFP. Arrowheads mark the location of MAG containing high complex oligosaccharides (a), mannose rich oligosaccharides (b) and the deglycosylated protein (containing only the core *N*-acetylglucosamines) (c). The location of molecular weight markers is shown in kDa on the right. **(C)** Differential recognition of the MAG-S133R mutant by specific antibodies. Fixed and permeabilized COS7 cells expressing the wild-type (*WT*) and mutant (*S133R*) forms of MAG were immunolabelled using the indicated antibodies. Note that MAb 513 does not recognize the mutant protein. Scale bars = 20 μm.

translational processing of MAG. Further analysis using endoglycosidase H (EndoH) revealed that while the wild-type protein contained highly processed complex oligosaccharides, MAG-S133R only contained immature asparagine-linked mannose-rich oligosaccharides (Fig. 3B). The presence of high mannose glycans in glycoproteins is an indication of endoplasmic reticulum retention and protein folding abnormalities (Helenius and Aebi, 2004). Immunolabelling of COS7 cells transfected with wild-type or mutant MAG using four different antibodies to MAG revealed that in contrast to monoclonal antibody (Mab) D3A2G5, which is directed to the extracellular portion of human MAG (Burger *et al.*, 1990), or polyclonal antibodies against the intracellular domain (Heape *et al.*, 1999), MAb 513 did not detect the mutant MAG-S133R (Fig. 3C). Given that the latter antibody recognizes a conformational epitope (Meyer-Franke *et al.*, 1995), these results further support the detrimental effect of the S133R mutation on folding of MAG. These results are in line with previous observations that N-linked glycosylation of MAG plays a role in its proper folding (Tropak *et al.*, 1997).

MAG-S133R mutant is trapped in the endoplasmic reticulum

Whereas wild-type transfected COS7 cells showed MAG present on the entire cell, MAG-S133R mutant was concentrated around the nucleus, suggesting that it does not reach the cell surface (Fig. 3C). To further determine whether this is the case, we immunolabelled live transfected COS7 cells using the MAb D3A2G5 (Fig. 4A). Unlike wild-type MAG, which was detected on the cell surface, MAG-S133R could only be detected in detergent-permeabilized cells. Similar distribution was detected in Schwann cells expressing MAG-GFP and MAG-S133R-GFP (Fig. 4B). Analysis of Schwann cells co-expressing MAG-MYC or MAG-S133R-MYC with farnesylated GFP that marks the plasma membrane (Rhee *et al.*, 2006) showed similar distribution (Fig. 4C). In addition, cell surface biotinylation of HEK293T cells expressing MAG-GFP and MAG-S133R-GFP using a membrane-impermeable reagent demonstrated that only wild-type MAG was detectable on the cell surface
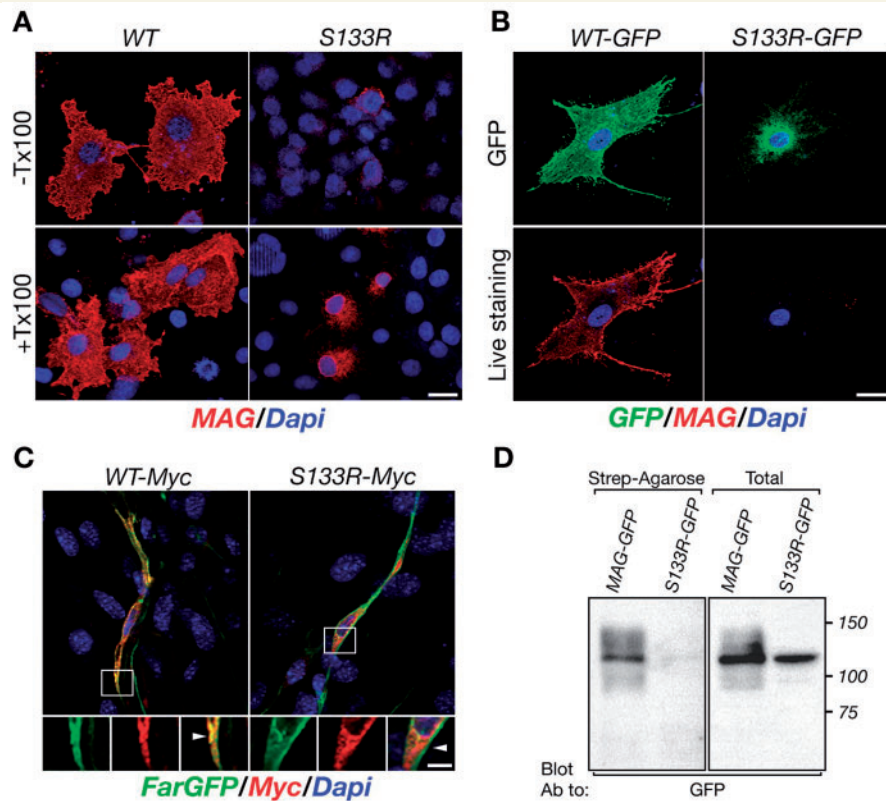
Figure 4 MAG-S133R does not reach the cell surface. (A) Cell surface expression of the wild-type (*WT*) and MAG-S133R (*S133R*) proteins in transfected COS7 cells. Cells were stained with the D3A2G5 antibody, which recognize the extracellular region of MAG, either without (-Tx100) or with (+Tx100) fixation and permeabilization. The cellular nuclei were labelled with DAPI (blue). **(B)** Distribution of MAG-GFP or MAG-S133R-GFP in transfected rat Schwann cells. **(C)** Distribution of MAG-MYC or MAG-S133-MYC co-infected with plasma membrane marker farnesylated GFP (FarGFP) in rat Schwann cells. Scale bars: **A–C** = 20 μm. **(D)** Cell surface expression of MAG-GFP and MAG-S133R-GFP proteins in MAG-GFP or MAG-S133R-GFP expressing HEK 293T cells. Surface proteins where labelled using impermeable NHS-sulfo biotin. Lysates were precipitated with streptavidin-conjugated agarose beads followed western blot analysis using antibodies to GFP. The location of molecular weight markers is shown in kDa on the right.

(Fig. 4D). Double immunolabelling of HeLa cells expressing wild-type or MAG-S133R using antibodies to MAG and to endoplasmic reticulum protein calnexin (encoded by *CANX*) (Ou *et al.*, 1993) or to the Golgi-associated protein p115 (encoded by *USO1*) (Waters *et al.*, 1992) showed that MAG-S133R is confined to the endoplasmic reticulum but does not co-localized with p115 (Fig. 5A and B). The mutant, but not the wild-type protein, co-localized with the endoplasmic reticulum protein vesicle-associated membrane protein-associated protein B/C (encoded by *VAPB*) (Peretti *et al.*, 2008) in both transfected COS7 (Fig. 5C) and rat Schwann cells (Fig. 5F). MAG-S133R also co-localized with CASPR, contactin-associated protein (encoded by *CNTNAP1*) (Fig. 5D), a transmembrane protein that requires the presence of contactin to exit the endoplasmic reticulum (Faivre-Sarrailh *et al.*, 2000; Gollan *et al.*, 2003). In addition, we found that when expressed in rat oligodendrocytes, MAG-S133R-GFP was also confined to the endoplasmic reticulum (Fig. 5E). Immunoprecipitation of MAG-GFP and MAG-S133R-GFP

from HEK293T cells revealed that unlike MAG, MAG-S133R co-immunoprecipitated with endoplasmic reticulum-resident glycan calnexin and endoplasmic reticulum chaperone 78 kDa glucose-regulated protein (Bip, encoded by *HSPA5*) (Gething, 1999) (Fig. 5G). These results demonstrate that MAG-S133R does not reach the cell surface and is stuck in the endoplasmic reticulum, further confirming the detrimental effect of the p.S133R mutation on the folding and processing of MAG.

MAG-S133R undergoes proteasome-dependent degradation

Endoplasmic reticulum accumulation of terminally misfolded proteins leads to their degradation (Meusser *et al.*, 2005). To examine whether endoplasmic reticulum-retained MAG-S133R is subject to degradation, we determined the half-life of MAG-MYC and MAG-S133R-MYC proteins in HEK293T cells using cyclohexamide chase assay (Fig. 6A and B). MAG-S133R-MYC displayed significantly higher
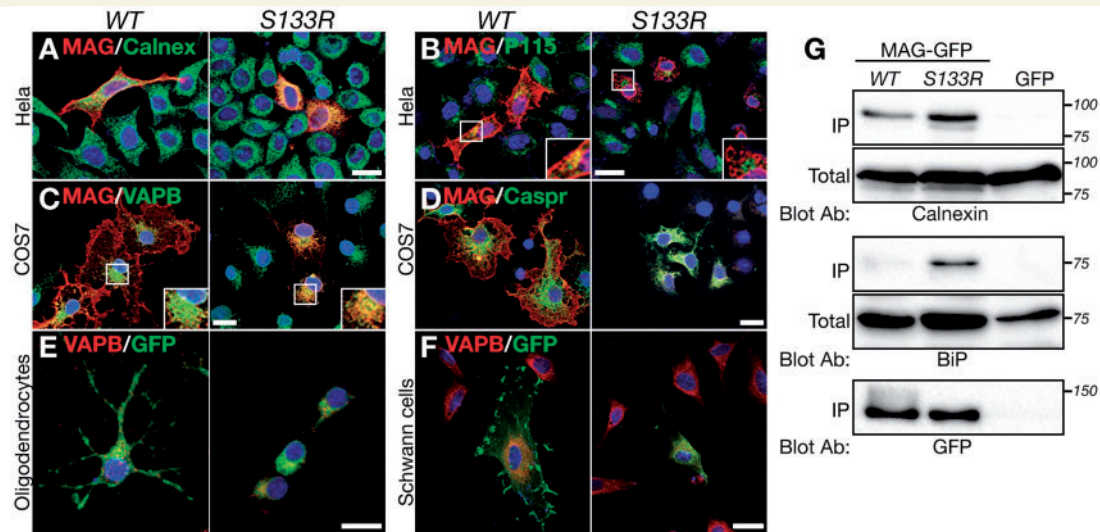
Figure 5 S133R MAG accumulates in the endoplasmic reticulum. (**A** and **B**) Hela cells expressing the wild-type (*WT*) or MAG-S133R (*S133R*) proteins were immunolabelled using an antibody to MAG and to calnexin (**A**), or to p115 (**B**). (**C** and **D**) COS7 cells expressing the wild-type (*WT*) or MAG-S133R (*S133R*) proteins were immunolabelled using an antibody to MAG and to the endoplasmic reticulum marker proteins VAPB (**C**) or Caspr (**D**). (**E**) Rat oligodendrocytes expressing MAG-GFP (*WT*) or MAG-S133R-GFP (*S133R*) were immunolabelled using an antibody to VAPB. (**F**) Rat Schwann cells expressing MAG-GFP (*WT*) or MAG-S133R-GFP (*S133R*) were immunolabelled using an antibody to VAPB. The GFP fluorescence is shown in green. Note that MAG-S133R is associated with endoplasmic reticulum markers. Scale bars = 20 μm. (**G**) MAG-S133R co-imunoprecipitation with endoplasmic reticulum proteins calnexin and BiP. HEK 293T expressing MAG-GFP and MAG-S133R-GFP where imunopercipitated using GFP antibody-conjugated beads and subjected to western blot analysis using antibodies to calnexin and BiP. The location of molecular weight markers is shown in kDa on the right.

degradation rate with a half-life of ∼2 h compared to a very stable MAG-MYC. Degradation rate of MAG-S133R was reduced by the addition of proteasome inhibitor bortezomib (Fig. 6C). In bortezomib-treated cells, MAG-S133R-GFP, but not MAG-GFP, was polyubiquitinated, indicating that it is destined to the proteasome for degradation (Fig. 6E). In addition, the fact that polyubiquitination of MAG-S133R-GFP could only be detected after proteasomal inhibition, further indicates that the mutant protein is rapidly degraded (Altier *et al.*, 2011). Immunoprecipitation of MAG-GFP and MAG-S133R-GFP in HEK293T cells showed that as opposed to wild-type protein, MAG-S133R was associated with components of the endoplasmic reticulum-associated protein degradation (ERAD) machinery, such as P97 (OS9, SEL1) (Christianson *et al.*, 2008) (Fig. 6D).

To determine what intracellular proteins are associated with the wild-type and the mutant protein, we subjected MAG-GFP and MAG-S133R-GFP immunocomplexes to high resolution mass spectrometry-based proteomic analysis. Statistical tests showed clear differences between interactors of wild-type MAG-GFP and MAG-S133R-GFP (Student *t*-test, FDR = 0.05, S0 = 1.5). Wild-type MAG was mainly associated with proteins related to the Golgi apparatus and protein glycosylation, consistent with its localization at the plasma membrane and its post-translational N-glycosylation modifications (Fig. 7). In contrast, MAG-S133R was associated with a number of endoplasmic reticulum processing proteins, such as BiP,

calnexin, calreticulin, PDIA3, and PDIA4, with proteins related to protein folding, such as the chaperonin-containing T-complex (Horwich and Willison, 1993), and with COP1 coating proteins, responsible for the retrograde transport from Golgi back to the endoplasmic reticulum (Spang and Schekman, 1998) (Fig. 7A and B). Finally, the mutant protein was associated with a number of ERAD proteins, such as P97, OS9, SEL1 and EDEM3, as well as with proteasomal proteins, such as PSMC1, PSMC4, PSMD1 and PSMD3 (Fig. 7B). Collectively, our results demonstrate that the p.S133R mutation affects the post-translational processing and folding of MAG, leading to its retention in the endoplasmic reticulum with subsequent ERAD-mediated proteasomal degradation.

Based on these results, we immunohistochemically stained sural nerve biopsy sample of Patient III-2 for MAG showing complete absence of myelin sheath staining (Fig. 2G).

Discussion

Using genetic linkage, exome sequencing and cellular expression studies, we identified a homozygous missense c.399 C > G; p.S133R mutation in *MAG* in a consanguineous multiplex family with PMD-like disorder. Affected siblings presented the typical for PMD developmental and motor delay of infantile-onset with early nystagmus and hypotonia slowly evolving into a form of complicated
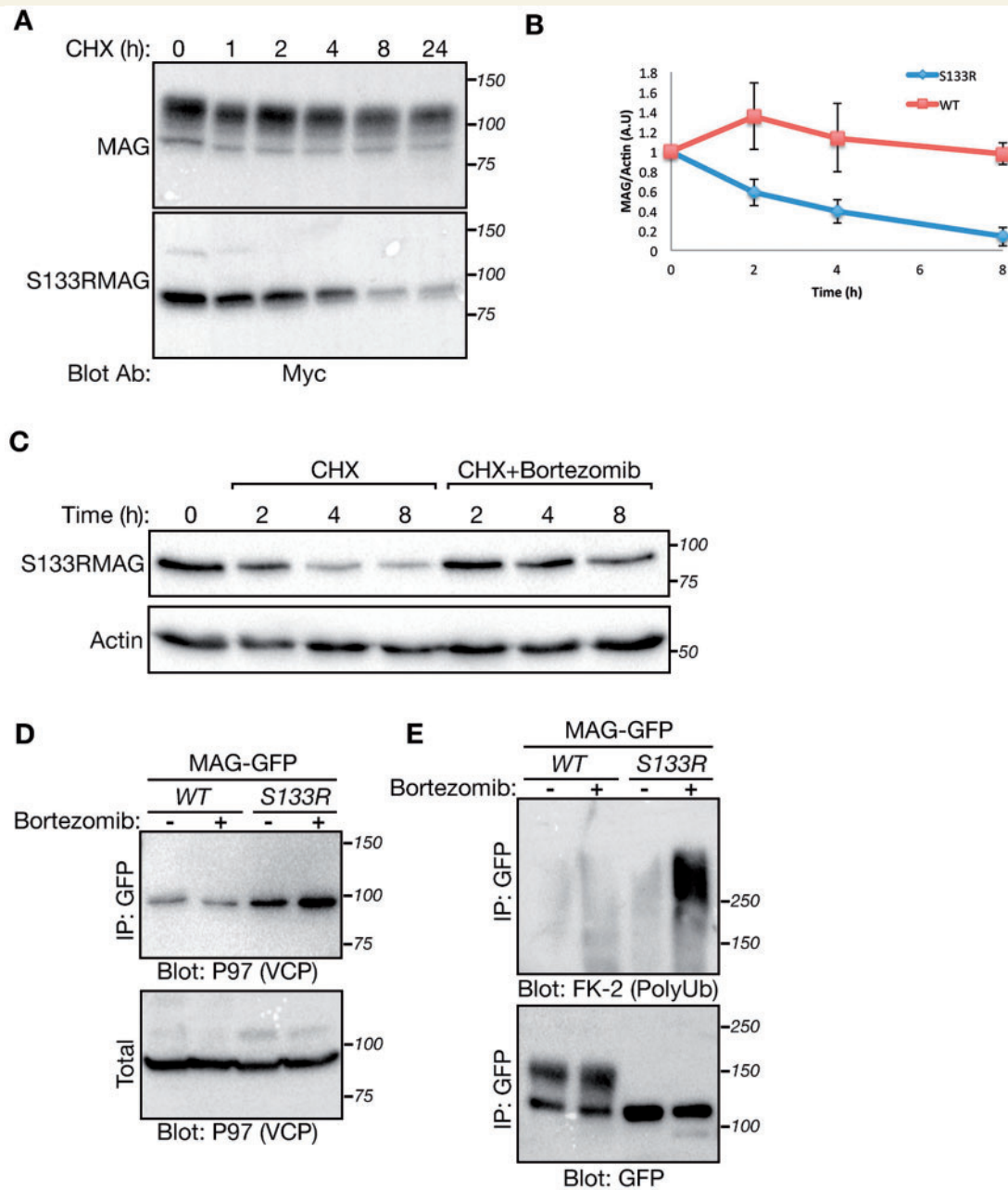
Figure 6 MAG-S133R undergoes proteasome dependent degradation and associates with ERAD machinery. (**A** and **B**) MAG-S133R degradation rate is higher than wild-type MAG. HEK293T expressing wild-type MAG-MYC and MAG-S133-MYC subjected to cyclohex-amide chase, at the indicated time points, total protein lysates were subjected to western blot analysis using MYC antibody. (**B**) Degradation rate plot analysis, MAG intensity relative to actin (image-lab software) from three independent experiments. (**C**) MAG-S133R degradation is prote-asome dependent. HEK293T expressing wild-type MAG-MYC and MAG-S133-MYC subjected to cyclohexamide chase with or without borte-zomib at the indicated time points, total protein lysates were subjected to western blot analysis using MYC antibody. (**D** and **E**) MAG-S133R associates with ERAD protein P97 and is polyubiquitinated. HEK293T expressing MAG-GFP and MAG-S133R-GFP where immunoprecipitation using GFP antibody conjugated beads and subjected to western blot analysis using P97 and FK-2 antibodies. The location of molecular weight markers is shown in kDa on the right.

HSP with mental retardation, dysarthria, optic atrophy and peripheral neuropathy in adulthood. The mild variability observed among the siblings likely results from age-related progression of the underlying process. Although HLD1, HLD2 and HLD4 also exhibit PMD-like and HSP pheno-types, the combination of clinical and imaging findings clearly distinguishes the disorder in this family from other forms (Supplementary Table 2).

As the PMD-like phenotype is associated with myelin-related genes *PLP1* and *GJC2* (Pouwels *et al.*, 2014), in-volvement of *MAG* in this family may not be surprising. The encoded protein MAG is a quantitatively minor
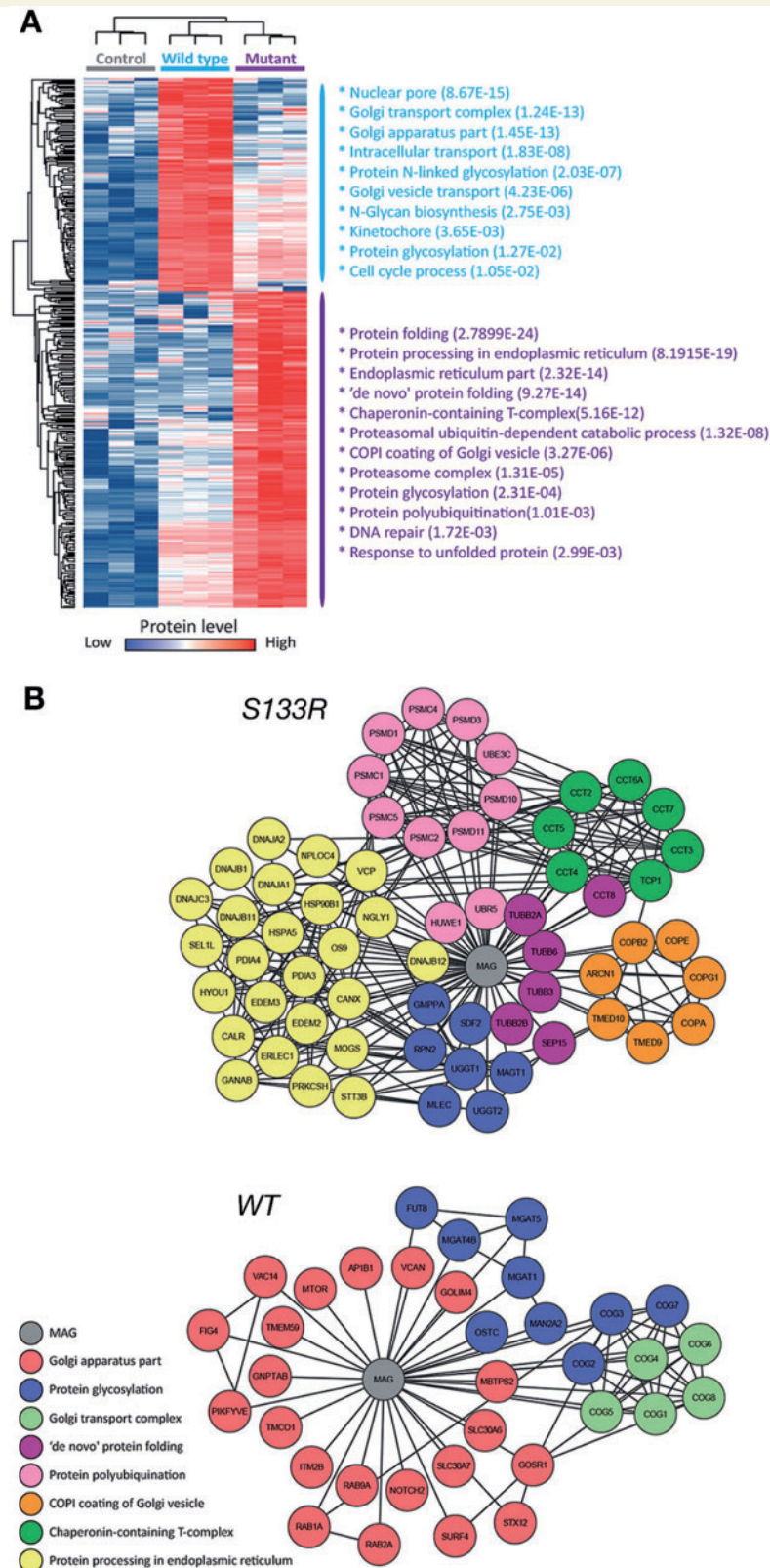
Figure 7 Mass spectrometry-based interaction proteomics. MAG and MAG-S133R associate with distinct protein interaction networks. (**A**) Hierarchical clustering of 423 significantly changing proteins between wild-type and mutant (Student *t*-test; FDR = 0.05; S0 = 1.5). Selected enriched categories (GOCC, GOBP and KEGG) based on Fisher exact test are shown on the right, followed by their FDR corrected q-value. (**B**) Interaction network of potential interaction partners of MAG wild-type (*lower map*) and MAG-S133R (*upper map*). The protein network was built using the string database. Colours are based on selected significantly enriched categories. MAG is at the centre of each map.

component of myelin and is expressed solely by oligo-dendrocytes and Schwann cells (Quarles, 2007), consistent with the combined CNS and PNS involvement in our patients. It is an adhesion molecule in the periaxonal layer of mature non-compact myelin membrane facing the axon. Based on its location and the fact that its expression correlates with the initiation of myelination (Quarles, 2007), MAG is thought to mediate interactions between myelinating glia and their underlying axons (Lopez, 2014).

MAG is a highly glycosylated transmembrane protein containing an extracellular segment with five tandem Ig-like domains (Quarles, 2007). The c.399C > G mutation identified in this family involves the first Ig-like domain and leads to a single amino acid substitution p.S133R, predicted to destabilize the protein, affect its glycosylation and cause defective folding. Accordingly, our studies demonstrate that the MAG-S133R mutant contains mannose-rich oligosaccharides instead of highly processed complex oligosaccharides, indicative of its endoplasmic reticulum retention (Helenius and Aebi, 2004). In line with the notion that N-linked glycosylation is important for proper folding (Tropak et al., 1997), MAG-S133R is not recognized by MAb 513, which recognizes conformational epitope (Meyer-Franke et al., 1995) of the wild-type protein. The MAG-S133R mutant is present in the endoplasmic reticulum in a variety of transfected cells, co-immunoprecipitating with the endoplasmic reticulum chaperones calnexin and calreticulin, known to increase the efficiency of glycoprotein folding and to ensure that misfolded proteins are retained in the endoplasmic reticulum (Rajagopalan et al., 1994). The mutant MAG also associates with the endoplasmic reticulum protein BiP (GRP78), which facilitates protein folding and regulates the unfolded protein response. Mass spectrometry-based proteomics corroborates our findings that MAG-S133R is retained in the endoplasmic reticulum. Furthermore, MAG-S133R interacts with proteins of the COP1 family, responsible for the retrograde transport of proteins from Golgi to endoplasmic reticulum, which likely prevents mutated MAG to proceed along the secretory pathway.

Cyclohexamide experiments reveal that MAG-S133R undergoes rapid degradation and removal, compared to the stable wild-type MAG. Moreover, this rapid degradation is proteasome-dependent. Consistent with this observation, MAG-S133R, but not the wild-type MAG, is polyubiquitinated and is associated with ERAD machinery proteins P97, OS9, SEL1 and EDEM3. Moreover, MAG-S133R directly associates with proteasomal subunits representative of the proteasome-dependent nature of degradation. It is also important to note that MAG-S133R does not induce the activation of endoplasmic reticulum stress mediators PERK, IRE1 and ATF6 endoplasmic reticulum. Collectively, our results suggest that the c.399C > G; p.S133R mutation in MAG leads to ERAD-mediated loss of the protein, which corresponds to the immunohistochemical absence of MAG in the sural nerve biopsy specimen of Patient III-2 (Fig. 2G).

Loss of tissue immmunoreactivity for MAG also characterizes genetically manipulated knockout mice (Li et al.,

1994; Montag et al., 1994). When examined by the age of 4 months, affected animals show surprisingly mild clinical and pathological alterations in the CNS and PNS, display normal peripheral nerve conduction, and are able to generate mature myelin. Delayed CNS myelination, redundant or disrupted compact myelin, oligodendroglial periaxonal area and cytoplasmic collar changes (Montag et al., 1994), tremor and impaired coordination (Li et al., 1994) are among the reported alterations at this stage (Lopez, 2014). Normal MRI myelination pattern in our patients in childhood (Patient III-2) and in adulthood is consistent with these findings and still leaves a possibility of delayed myelination in infancy to explain their early PMD-like manifestations.

At a later age, additional alterations are described in MAG knockout animals, including degeneration of axons and myelin in the PNS accompanied by the formation of onion bulb-like structures (Fruttiger et al., 1995). Peripheral nerve conduction studies show reduced velocities with a less significantly decreased compound muscle action potential amplitudes (Weiss et al., 2001). These abnormalities qualitatively resemble electron microscopic findings in Patient III-2 (Fig. 2) and an apparent age-related worsening of the peripheral nerve conduction findings between siblings, Patients III-5, III-3 and III-2 (Supplementary Table 1).

Long-term alterations in the CNS in MAG knockout animals include axonal degeneration (Nguyen et al., 2009) and dying-back oligodendrogliopathy, which possibly represents initial stages of a slow demyelinating process (Lassmann et al., 1997). Clinical and electrophysiological signs of the CNS involvement in our patients in adulthood accompanied by the cerebral MRI and ^{1}H-magnetic resonance spectroscopy abnormalities (Supplementary Table 1 and Fig. 1E) are also indicative of a demyelinating form of leukodystrophy. Taken together, our findings confirm a slowly progressive involvement of the PNS and CNS in this family with c.399C > G mutation in MAG and are consistent with the suggested function of MAG in a long-term maintenance and integrity of myelin and axons (Lopez, 2014).

Recently, another mutation in MAG has been reported in a monumental study of multiple HSP families (Novarino et al., 2014). The two affected sisters carrying the c.1288T > G; p.C430G mutation in the core of the fifth Ig-like domain, manifested early-onset HSP associated with nystagmus, cerebellar signs, amyotrophy, sensory loss and poor school achievements, akin to the late clinical phenotype in our patients. Although their MRI was tabulated as normal, no details, ^{1}H-magnetic resonance spectroscopy or nerve conduction results were available for comparison.

In summary, we provide the first conclusive evidence for the involvement of MAG in a combined CNS and PNS disorder manifesting early PMD-like clinical phenotype later evolving into a complicated HSP. Given autosomal recessive inheritance in this family, we postulate that the underlying mechanism of the p.S133R mutation is related to the ERAD-mediated loss of MAG function. Because MAG is developmentally regulated through alternative

mRNA splicing of the cytoplasmic domain generating short and long isoforms differentially expressed in the PNS and CNS, it is conceivable that MAG is responsible for a broader range of neurogenetic disorders.

Supplementary material

Supplementary material is available at *Brain* online.

References

Altier C, Garcia-Caballero A, Simms B, You H, Chen L, Walcher J, et al. The Cavbeta subunit prevents RFP2-mediated ubiquitination and proteasomal degradation of L-type channels. Nat Neurosci 2011; 14: 173–80.

Bizzi A, Castelli G, Bugiani M, Barker PB, Herskovits EH, Danesi U, et al. Classification of childhood white matter disorders using proton MR spectroscopic imaging. AJNR Am J Neuroradiol 2008; 29: 1270–5.

Burger D, Simon M, Perruisseau G, Steck AJ. The epitope(s) recognized by HNK-1 antibody and IgM paraprotein in neuropathy is present on several N-linked oligosaccharide structure on human P0 and myelin-associated glycoprotein. J Neurochem 1990; 54: 1569–75.

Christianson JC, Shaler TA, Tyler RE, Kopito RR. OS-9 and GRP94 deliver mutant alpha 1-antitrypsin to the Hrd1-SEL1L ubiquitin ligase for ERAD. Nat Cell Biol 2008; 10: 272–82.

Cox J, Neuhauser N, Michalski A, Scheltema RA, Olsen JV, Mann M. Andromeda: a peptide search engine integrated into the MaxQuant environment. J Proteome Res 2011; 10: 1794–805.

Cox J, Hein MY, Luber CA, Paron I, Nagaraj N, Mann M. Accurate proteome-wide label-free quantification by delayed normalization and maximal peptide ration extraction, termed MaxLFQ. Mol Cell Proteomics 2014; 13: 2513–26.

Erb M, Steck AJ, Nave KA, Schaeren-Wiemers N. Differential expression of L- and S-MAG upon cAMP stimulated differentiation in oligodendroglial cell. J Neurosci Res 2003; 71: 326–37.

Eshed Y, Feiberg K, Poliak S, Sabanay H, Sarig-Nadir O, Spiegel I, et al. Gliomedin mediates Schwann cell-axon interaction and the molecular assembly of the nodes of Ranvier. Neuron 2005; 47: 215–29.

Faivre-Sarrailh C, Gauthier F, Denisenko-Nehrbass N, Le Bivic A, Rougon G, Girault JA. The glycosylphosphatidyl inositol-anchored adhesion molecule F3/contactin is required for surface transport of paranodin/contactin-associated protein (caspr). J Cell Biol 2000; 149: 491–502.

Feinstein M, Markus B, Noyman I, Shalev H, Flusser H, Shelef I, et al. Pelizaeus-Merzbacher-like disease caused by AIMP1/p43 homozygous mutation. Am J Hum Genet 2010; 87: 820–8.

Folstein MF, Folstein SE, McHugh PR. "Mini-mental state". A practical method for grading the cognitive state of patients for the clinician. J Psychiatr Res 1975; 12,189–98.

Fruttiger M, Montag D, Schachner M, Martini R. Crucial role for the myelin-associated glycoprotein in the maintenance of axon-myelin integrity. Eur J Neurosci 1995; 7: 511–5.

Gething MJ. Role and regulation of the ER chaperon BiP. Semin Cell Dev Biol 1999; 10: 465–72.

Gollan L, Salomon D, Salzer JL, Peles E. Caspr regulates the processing of contactin and inhibits its binding to neurofascin. J Cell Biol 2003; 163: 1213–8.

Han H, Myllykoski M, Ruskamo S, Wang C, Kursula P. Myelin-specific proteins: a structurally diverse group of membrane-interacting molecules. Biofactors 2013; 39: 233–41.

Heape AM, Lehto VP, Kursula P. The expression of recombinant large myelin-associated glycoprotein cytoplasmic domain and the purification of native myelin-associated glycoprotein from rat brain and peripheral nerve. Protein Expr Purif 1999; 15: 349–61.

Helenius A, Aebi M. Roles of N-linked glycans in the endoplasmic reticulum. Annu Rev Biochem 2004; 73: 1019–49.

Henneke M, Combes P, Diekmann S, Bertini E, Brockmann K, Burlina AP, et al. GJA12 mutations are a rare cause of Pelizaeus-Merzbacher-like disease. Neurology 2008; 70: 748–54.

Hobson GM, Garbern JY. Pelizaeus-Merzbacher disease, Pelizaeus-Merzbacher-like disease 1, and related disorders. Semin Neurol 2012; 32: 62–7.

Horwich AL, Willison KR. Protein folding in the cell: functions of two families of molecular chaperon, hsp 60 and TF55-TCP1. Phil Trans R Soc Lond Biol Sci 1993; 339: 313–25; discussion 25–6.

Lassmann H, Bartsch U, Montag D, Schachner M. Dying-back oligodendrogliopathy: a late sequel of myelin-associated glycoprotein deficiency. Glia 1997; 19: 104–10.

Letunic I, Doerks T, Bork P. SMART 7: recent updates to the protein domain annotation resource. Nucleic Acids Res 2012; 40: D302–5.

Li C, Tropak MB, Gerlai R, Clapoff S, Abramow-Newerly W, Trapp B, et al. Myelination in the absence of myelin-associated glycoprotein. Nature 1994; 369: 747–50.

Lopez PHH. Role of myelin-associated glycoprotein (siglec-4A) in the nervous system. Adv Neurobiol 2014; 9: 245–62.

Magen D, Georgopoulos C, Bross P, Ang D, Segev Y, Goldsher D, et al. Mitochondrial Hsp60 chaperonopathy causes an autosomal-recessive neurodegenerative disorder linked to brain hypomyelination and leukodystrophy. Am J Hum Genet 2008; 83: 30–42.

May AP, Robinson RC, Vinson M, Crocker PR, Jones EY. Crystal structure of the N-terminal domain of sialoadhesin in complex with 3' sialyllactose at 1.85 A resolution. Mol Cell 1998; 1: 719–28.

Meyer-Franke A, Tropak MB, Roder JC, Fischer P, Beyreuther K, Probstmeier R, et al. Functional topography of myelin-associated glycoprotein. II. Mapping of domains on molecular fragments. J Neurosci Res 1995; 41: 311–23.

Meusser B, Hirsh C, Jarosch E, Sommer T. ERAD: the long road to destruction. Nat Cell Biol 2005; 7: 766–72.

Miyatake S, Osaka H, Shiina M, Sasaki M, Takanashi J, Haginoya K, et al. Expanding the phenotypic spectrum of TUBB4A-associated hypomyelinating leukodystrophies. Neurology 2014; 82: 2230–37.

Montag D, Giese KP, Bartsch U, Martini R, Lang Y, Bluthmann H, et al. Mice deficient for the myelin-associated glycoprotein show subtle abnormalities in myelin. Neuron 1994; 13: 229–46.

Nguyen T, Mehta NR, Conant K, Kim K-J, Jones M, Calabresi PA, et al. Axonal protective effects of the myelin-associated glycoprotein. J Neurosci 2009; 29: 630–7.

Novarino G, Fenstermaker AG, Zaki MS, et al. Exome sequencing links corticospinal motor neuron disease to common neurodegenerative disorders. Science 2014; 343: 506–11.

Orthmann-Murphy JL, Salsano E, Abrams CK, Bizzi A, Uziel G, Freidin MM, et al. Hereditary spastic paraplegia is a novel phenotype for GJA12/GJC2 mutations. Brain 2009; 132: 426–38.

Ou WJ, Cameron PH, Thomas DY, Bergeron JJ. Association of folding intermediates of glycoproteins with calnexin during protein maturation. Nature 1993; 364: 771–6.

Peles E, Nativ M, Lustig M, Grumet M, Schilling J, Martinez R, et al. Identification of a novel contactin-associated transmembraine receptor with multiple domains implicated in protein-protein interactions. Embo J 1997; 16: 978–88.

Peretti D, Dahan N, Shimoni E, Hirschberg K, Lev S. Coordinated lipid transfer between the endoplasmic reticulum and the Golgi complex requires the VAP proteins and is essential for Golgi-mediated transport. Mol Biol Cell 2008; 19: 3871–84.

Pouwels PJW, Vanderver A, Bernard G, Wolf NI, Dreha-Kulczewksi SF, Deoni SCL, et al. Hypomyelinating leukodystrophies: translational research progress and prospects. Ann Neurol 2014; 76: 5–19.

Quarles RH. Myelin-associated glycoprotein (MAG): past, present and beyond. J Neurochem 2007; 100: 1431–48.

Rajagopalan S, Xu Y, Brenner MB. Retention of unassembled components of integral membrane proteins by calnexin. Science 1994; 263: 387–90.

Rhee JM, Pirity MK, Lackan CS, Long JZ, Kondoh G, Takeda J, et al. *In vivo* imaging and differential localization of lipid-modified GFP-variant fusions in embryonic stem cells and mice. Genesis 2006; 44: 202–18.

Roy A, Kucukural A, Zhang Y. I-TASSER: a unified platform for automated protein structure and function prediction. Nat Protoc 2010; 5: 725–38.

Shimojima K, Okumura A, Ikeno M, Nishimura A, Saito A, Saitsu H, et al. A *de novo* TURBB4A mutation in a patient with hypomyelination mimicking Pelizaeus-Merzbacher disease. Brain Dev 2015; 37: 281–5. 10.1016/j.braindev.2014.05.004

Seelow D, Schuelke M, Hildebrandt F, Nürnberg P. HomozygosityMapper-an interactive approach to homozygosity mapping. Nucleic Acids Res 2009; 37: W593–9.

Söding J. Protein homology detection by HMM-HMM comparison. Bioinformatics 2005; 21: 951–60.

Spang A, Schekman R. Reconstitution of retrograde transport from Golgi to the ER *in vitro*. J Cell Biol 1998; 143: 589–99.

Spiegel I, Adamsky K, Eshed Y, Milo R, Sabanay H, Sarig-Nadir O, et al. A central role for Necl4 (SynCAM4) in Schwann cell-axon interaction and myelination. Nat Neurosci 2007; 10: 861–9.

Tropak MB, Roder JC. Regulation of myelin-associated glycoprotein binding by sialylated cis-ligands. J Neurochem 1997; 68: 1753–63.

Vaurs-Barriere C, Deville M, Sarret C, Giraud G, Des Portes V, Prats-Vinas J-M, et al. Pelizaeus-Merzbacher-like disease presentation of MCT8 mutated male subjects. Ann Neurol 2009; 65: 114–8.

Waters MG, Clary DO, Rothman JE. A novel 115-kD peripheral membrane protein is required for intercisternal transport in the Golgi stack. J Cell Biol 1992; 118: 1015–26.

Weiss MD, Luciano CA, Quarles RH. Nerve conduction abnormalities in aging mice deficient for myelin-associated glycoprotein. Muscle Nerve 2001; 24: 1380–7.